Earthq Eng & Eng Vib (2016) 15: 617-626 **DOI**:10.1007/s11803-016-0348-7

Seismic damage analysis of the outlet piers of arch dams using the finite element sub-model method

Song Liangfeng[1, 2†], Wu Mingxin[1‡], Wang Jinting[1§] and Xu Yanjie[1*]

1. *State Key Laboratory of Hydroscience and Engineering, Tsinghua University, Beijing 100084, China*

2. *Three Gorges International Tendering Co. Ltd., Beijing 100038, China*

Abstract: This study aims to analyze seismic damage of reinforced outlet piers of arch dams by the nonlinear finite element (FE) sub-model method. First, the dam–foundation system is modeled and analyzed, in which the effects of infinite foundation, contraction joints, and nonlinear concrete are taken into account. The detailed structures of the outlet pier are then simulated with a refined FE model in the sub-model analysis. In this way the damage mechanism of the plain (unreinforced) outlet pier is analyzed, and the effects of two reinforcement measures (i.e., post-tensioned anchor cables and reinforcing bar) on the dynamic damage to the outlet pier are investigated comprehensively. Results show that the plain pier is damaged severely by strong earthquakes while implementation of post-tensioned anchor cables strengthens the pier effectively. In addition, radiation damping strongly alleviates seismic damage to the piers.

Keywords: arch dam; outlet pier; seismic damage; reinforcement measure; FE sub-model method

1 Introduction

Several arch dams over the height of 200 m are being built in Southwest China, a region with abundant water power but high seismic hazard. For these dams, outlet structures are usually arranged in the dam body to discharge water of great volume. Therefore, seismic behavior of outlet structures is an important issue in evaluating seismic safety of arch dams.

Many numerical models have been developed to analyze seismic response of arch dams in the last three decades. Several major influential factors, including dynamic dam–water–foundation interaction, opening and closing of contraction joints, reinforcement of contraction joints, concrete damage evolution, concrete aging, reservoir sediments, non-uniform seismic input, etc., have been investigated extensively (Chopra, 2012; Zhang and Jin, 2008; Wang *et al*., 2013; Alembagheri and Ghaemian, 2013; Bayraktar *et al*., 2011; Hariri-Ardebili and Mirzabozorg, 2013; Mircevska *et al*., 2014; Zhong *et al*., 2011). These efforts considerably improve understanding on the seismic behavior of arch dams. However, few investigations have been conducted to analyze the response of outlet structures to strong earthquakes. Li *et al*. (2013) investigated the effects of outlets and their piers on the seismic response of the Xiluodu dam. The nonlinear effect of contraction joints was considered in their investigation, but dam concrete was assumed to be linear elastic. They concluded that piers hinged to the dam body markedly affect stress distribution in the local region; however, their effect on the dynamic response of the dam body is insignificant.

In general, outlet piers are significantly small relative to the entire dam body. The element mesh of the dam body must be extra fine to simulate the detailed structures of outlet piers, and the total degrees-of-freedom (DOF) of the analysis model is significantly large; the cost of computation rises exponentially or becomes unaffordable. The finite element (FE) sub-model method aims to study a local region with a refined mesh along with a global model with coarse mesh. The FE sub-model analysis is useful in obtaining an accurate solution to a local region of structures and has been widely used in various fields (Bogdanovich and Kizhakkethara, 1999; Ciptokusumo *et al*., 2009; Giglio, 1999; Krishnan *et al*., 2008; Kuntiyawichai and Burdekin, 2003; Lucht, 2009). The FE sub-model has also been used in the dynamic analysis of outlet piers because of its efficiency in analyzing details of the structures. Li *et al.* (2008) performed a linear dynamic analysis of an arch dam outlet. Song *et al*. (2014) investigated dynamic damage in a local region of a concrete dam and verified the efficiency of the FE sub-model method for nonlinear

Correspondence to: Wang Jinting, Department of Hydraulic Engineering, Tsinghua University, Beijing 100084, China
Tel: +86-10-6278-3165; Fax: +86-10-6278-2159
E-mail: wangjt@tsinghua.edu.cn
†Master; ‡ PhD; §Professor; *Associate Professor

Supported by: National Natural Science Foundation of China under Grant Nos. 51179093 and 91215301, and Specialized Research Fund for the Doctoral Program of Higher Education under Grant No. 20130002110032

Received March 25, 2015; **Accepted** June 23, 2015

analysis.

Following Song *et al*. (2014), this study focuses on seismic damage of the reinforced outlet piers in arch dams. The detailed structures of the outlet piers are accurately simulated by the FE sub-model method. A 210-m-high arch dam that is being constructed in China is used as an analysis example. The commercial FE software ABAQUS (Dassault Systèmes Simulia, 2009) is employed to implement the numerical simulation. The global model considers the radiation damping of the infinite foundation, the opening of the contraction joints, and the dynamic damage of the dam concrete. The sub-model region, which is extracted from the global model, precisely simulates the detailed structures of an outlet pier by rebuilding an FE simulation. The failure mechanism of the plain outlet pier is analyzed, and the effects of two reinforcement measures, i.e., post-tensioned anchor cables and reinforcing bar, on the dynamic damage to the outlet pier are investigated comprehensively.

2 Computational model of the sub-model region

In this investigation, the global dam–reservoir–foundation system is analyzed by the nonlinear analysis model presented by Pan *et al.* (2009), in which the contraction joint is simulated by a contact boundary; the strain softening property of concrete is modeled by a plastic-damage model (Lee and Fenves, 1998); radiation damping of the infinite foundation is simulated by a viscous-spring artificial boundary condition (Liu and Li, 2005) at the truncated foundation boundary; and hydrodynamic pressure is represented by the added mass model for simplicity following current practice of design and research (FERC, 1999). For other modeling details, see Wang *et al*. (2013) and Pan *et al*. (2009). The following subsections present the computational model of the sub-model region.

2.1 Numerical simulation procedure

The procedure for the dynamic FE sub-model analysis is illustrated in Fig. 1. The coarse global model is initially analyzed and the dynamic responses at the driven nodes on the interface are determined. Subsequently, the fine sub-model is rebuilt and analyzed. Its boundary condition is defined based on the dynamic responses at the driven nodes in the global model. This means that the effect of the detailed changes of the sub-model region on the dynamic response of the global model is neglected in the sub-model analysis.

The equations of motion of the sub-model region nodes are:

$$\begin{bmatrix} \boldsymbol{K}_{\mathrm{ii}} & \boldsymbol{K}_{\mathrm{ib}} \\ \boldsymbol{K}_{\mathrm{bi}} & \boldsymbol{K}_{\mathrm{bb}} \end{bmatrix} \begin{Bmatrix} \boldsymbol{u}_{\mathrm{i}} \\ \boldsymbol{u}_{\mathrm{b}} \end{Bmatrix} + \begin{bmatrix} \boldsymbol{C}_{\mathrm{ii}} & \boldsymbol{C}_{\mathrm{ib}} \\ \boldsymbol{C}_{\mathrm{bi}} & \boldsymbol{C}_{\mathrm{bb}} \end{bmatrix} \begin{Bmatrix} \dot{\boldsymbol{u}}_{\mathrm{i}} \\ \dot{\boldsymbol{u}}_{\mathrm{b}} \end{Bmatrix} + \begin{bmatrix} \boldsymbol{M}_{\mathrm{ii}} & \boldsymbol{M}_{\mathrm{ib}} \\ \boldsymbol{M}_{\mathrm{bi}} & \boldsymbol{M}_{\mathrm{bb}} \end{bmatrix} \begin{Bmatrix} \ddot{\boldsymbol{u}}_{\mathrm{i}} \\ \ddot{\boldsymbol{u}}_{\mathrm{b}} \end{Bmatrix} = \begin{Bmatrix} \boldsymbol{F}_{\mathrm{i}} \\ \boldsymbol{F}_{\mathrm{b}} + \boldsymbol{r}_{\mathrm{b}} \end{Bmatrix} \tag{1}$$

where $\boldsymbol{M}$, $\boldsymbol{C}$ and $\boldsymbol{K}$ are the mass, damping and stiffness matrices, respectively; $\boldsymbol{F}$ is the external force vector; $\boldsymbol{r}$ represents the interaction force vector at the boundary interface; and subscripts i and b denote internal and boundary nodes, respectively.

Equation (1) is solved based on the external force vector $\boldsymbol{F}_{\mathrm{i}}$ and the boundary conditions (the specified displacement vector $\boldsymbol{u}_{\mathrm{b}}$) of the sub-model. For boundary nodes in the refined sub-model that do not coincide with the driven nodes, boundary displacement is determined by interpolating the dynamic solution of the global model as follows (Mao *et al*., 2001):

$$\boldsymbol{u}_{\mathrm{b}}(t) = \sum_{j=1}^{n} N_j \boldsymbol{u}_j(t) \tag{2}$$

where N_j is the shape function of the element in the coarse global model; $\boldsymbol{u}_j(t)$ is the displacement vector at driven node j; and t is the time variable.

Based on the aforementioned concept, the sub-model analysis procedure can be summarized by the following steps: (1) the global model with a coarse mesh is analyzed and the dynamic responses at the driven nodes are saved; (2) the FE model of the sub-model region is rebuilt and discretized with a fine mesh; (3) the original external loads are applied to the sub-model region; (4) the dynamic displacements at the boundary nodes of the sub-model are computed by interpolating the dynamic responses at the driven nodes of the global model; and (5) FE sub-model analysis is performed.

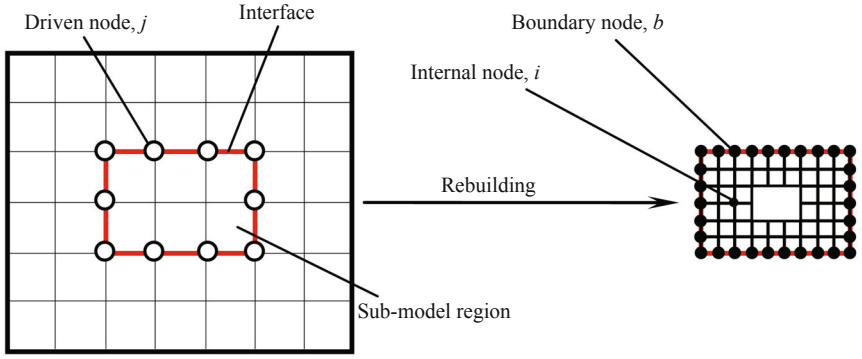

Fig. 1 Schematic of the FE sub-model method

2.2 Damage model of concrete

Excessive tensile stresses may lead to cracking of the outlet piers during strong earthquakes. Thus, nonlinear damage should be considered in the seismic analysis of concrete piers. Following the global analysis model used in this investigation, the sub-model analysis adopts the plastic-damage model (Lee and Fenves, 1998) to simulate the nonlinearity of the concrete material during strong earthquakes.

The compressive strength of concrete is significantly higher than its tensile strength. Thus, tensile damage of concrete is the most important issue in seismic safety evaluation of dams. Therefore, only tensile damage of concrete is considered in this study for simplicity. Moreover, compressive stiffness is assumed to fully recover upon the closure of cracks when load changes from tension to compression. Based on these assumptions, the uniaxial stress–strain relationship of concrete is shown in Fig. 2, where σ and ε are concrete stress and strain, respectively; E_0 is the initial (undamaged) elastic modulus; d_t is the tensile damage factor that varies from 0 (undamaged material with elastic behavior) to 1 (fully damaged material); G_f is the fracture energy; f_t is the tensile strength; ε_t and ε_f are the maximum elastic and limiting tensile strains, respectively; ε_p is the equivalent plastic strain; and l_c is the characteristic length of concrete (commonly defined as three times the maximum aggregate size).

2.3 Reinforced steel model without bond slip

The reinforcing bar in concrete is specified by the cross-section area of each rebar, the rebar spacing, and the rebar orientation. For convenience, the reinforcing bar is herein treated as a smeared layer with a constant thickness equal to the area of each rebar divided by the spacing, and simulated by membrane elements. By the embedded element technique, provided in ABAQUS, the membrane elements are embedded in a group of host concrete elements, as shown in Fig. 3. The nodal DOFs of the embedded membrane elements are constrained to the interpolated values of the corresponding DOFs of the host concrete elements.

Material properties of the rebar are defined separately

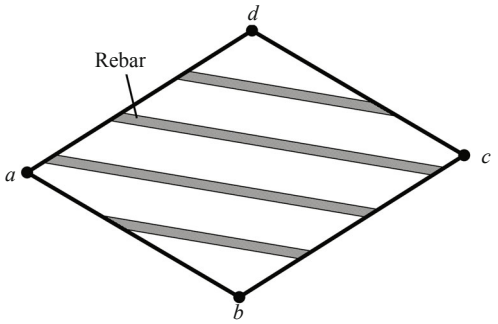

(a) Membrane element for rebar

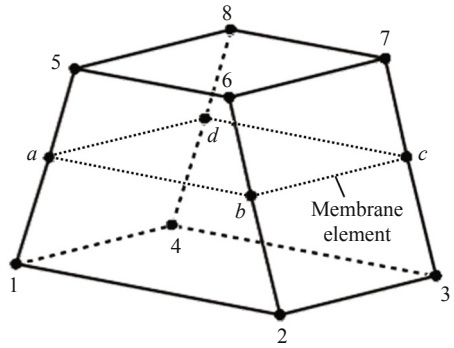

(b) Host concrete element embedding membrane element

Fig. 3 Simulation of reinforcing bar

from those of the host concrete. To take into account the contact effect between the steel and the concrete, a reinforced steel model without bond slip (Long *et al*., 2008) is adopted in this study. The stiffness contribution from steel–concrete interaction is simulated by stiffening the reinforcement. The reinforced tensile stress–strain relation of the rebar is shown in Fig. 4 and is formulated as follows:

$$\sigma^{s}=\begin{cases} E^{s}\varepsilon & 0\le\varepsilon<\varepsilon_{t} \\ 0.5\left[E^{s}\varepsilon+\sqrt{\left(E^{s}\varepsilon\right)^{2}+4af_{scr}^{2}}\right]-\dfrac{1-\rho}{\rho}\dfrac{\varepsilon-\varepsilon_{f}}{\varepsilon_{t}-\varepsilon_{f}} & \varepsilon_{t}\le\varepsilon<\varepsilon_{f} \\ 0.5\left[E^{s}\varepsilon+\sqrt{\left(E^{s}\varepsilon\right)^{2}+4af_{scr}^{2}}\right] & \varepsilon_{f}\le\varepsilon<\varepsilon_{y} \\ f_{y} & \varepsilon_{y}<\varepsilon \end{cases} \tag{3}$$

where σ^s is the rebar stress; ε_y represents the yielding

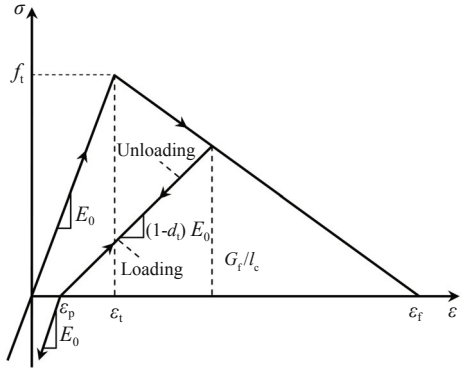

Fig. 2 Softening curve of concrete under uniaxial cyclic loading

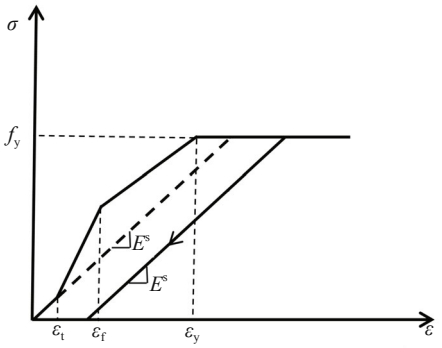

Fig. 4 Tensile stress–strain relations for the modified embedded steel model

strain of rebar at the cracking section; ρ is the rebar ratio; E^s is the elastic modulus of rebar; and

$$a=\sqrt{(1-\rho)/(1-\rho+n\rho)}\ ,\ f_{scr}=(1/\rho-1+n)f_t\ ,$$

$$n=E^s/E_0\ .$$

2.4 Embedded truss element model of anchor cables

We adopt the two-node 3D truss element (only bears axial tensile stress) provided by ABAQUS to simulate the post-tensioned anchor cables. Each anchor cable is discretized into a sequence of truss elements and embedded in solid concrete elements.

3 FE sub-model of the outlet pier

A 210-m-high arch dam, which is being constructed in China, is used as an example in this study. Seismic damage in one of its low-level outlets is investigated.

3.1 FE discretization

The global FE model of the arch dam with 28 contraction joints is shown in Fig. 5. The dam–foundation model is composed of 37,120 solid elements and 54,053 nodes. The dam has 26,235 solid elements, whose characteristic length is 2 m in the vertical direction. The four low-level outlets are considered in the global model, but their details are neglected. Outlet No.1 is selected as the research object.

Figure 6 shows the FE sub-model of outlet No.1 and its pier. The detail structures of the pier including the sidewall and crossbeam, and the reinforcement measures including the post-tensioned anchor cables and the reinforcing bar are accurately simulated. The sub-model has 12,344 3-dimensional solid elements and 15,025

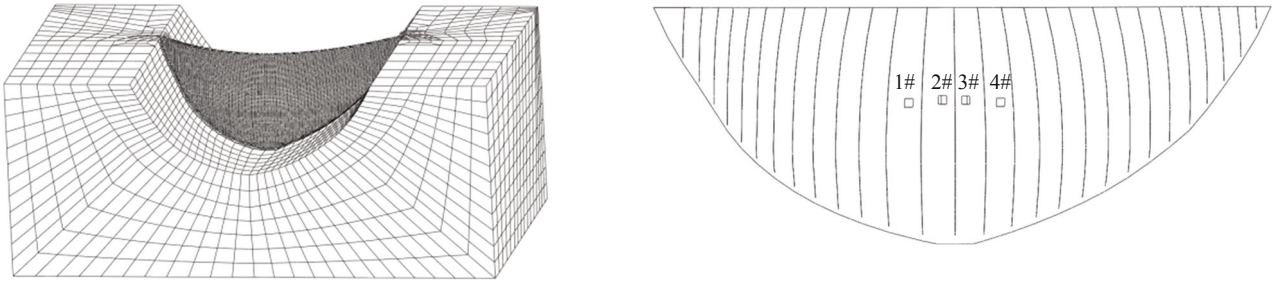

(a) FE discretization (b) Contraction joints and low-level outlets

Fig. 5 Global model of the analyzed dam–foundation system

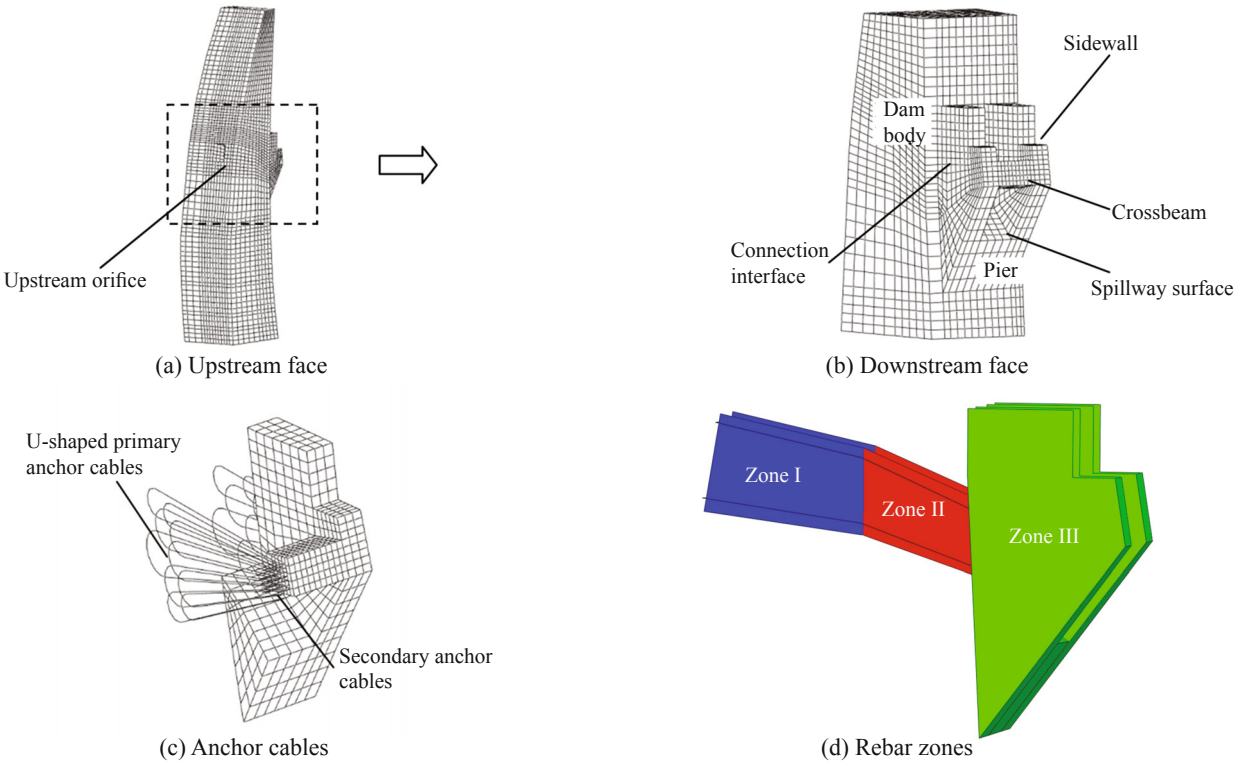

(a) Upstream face (b) Downstream face

(c) Anchor cables (d) Rebar zones

Fig. 6 FE sub-model of the outlet and its pier

nodes in total for concrete (Fig. 6(a)). The characteristic length of the elements is 1 m in the vertical direction. Fig. 6(c) shows the post-tensioned anchor cables, including 20 U-type primary anchor cables and 17 secondary anchor cables. Each primary anchor cable has 3,500 kN tension force and each secondary anchor cable has 2,500 kN tension force. These anchor cables are discretized as 849 2-node 3-dimensional truss elements. Fig. 6(d) shows the three rebar reinforcement zones, in which 2-layer Φ28@200 rebar in axis direction and 2-layer Φ36@200 rebar in annular direction are set in Zone I; 3-layer Φ28@200 rebar in axis direction and 3-layer Φ36@200 rebar in annular direction are set in Zone II; and single-layer Φ28@200 rebar in horizontal direction and single-layer Φ36@200 rebar in vertical direction are set in Zone III. Membrane elements are embedded into the sub-model to simulate the designed rebar.

3.2 Material parameters

Material properties of concrete, foundation rock, post-tensioned anchor cable, and reinforcing steel used in this study are selected mainly based on design data. The material properties are defined as follows: (1) for the dam concrete, mass density = 2,400 kg/m^3, initial dynamic elastic modulus = 31.2 GPa, and Poisson's ratio = 0.17; (2) for the foundation rock, density = 2,650 kg/m^3, elastic modulus = 26 GPa, and Poisson's ratio = 0.25; (3) for the steel strand of the post-tensioned anchor cables, density = 7,850 kg/m^3, elastic modulus = 195 GPa, and Poisson's ratio = 0.3; and (4) for the reinforcing steel: density = 7,850 kg/m^3, elastic modulus = 260 GPa, and Poisson's ratio = 0.3.

A nonlinear strain–softening constitutive relation shown in Fig. 2 is adopted for the dam to describe plastic–damage behavior of concrete. Tensile strength f_t of concrete used in the analysis is 3.12 MPa. Fracture energy G_f is 280 N/m based on experience. The limiting tensile strain ε_f is set to be 400 mm, and the characteristic length l_c is 0.45 m (Wang *et al*., 2000).

Material damping of the dam–foundation system is assumed to be of Rayleigh type. According to China Specification of Seismic Design of Hydraulic Structures (DL5073-2000, 2000), the damping ratio used in the first and fifth vibration modes of the dam–foundation system is 5%. Radiation damping of the foundation rock is simulated by the viscous-spring artificial boundary model (Pan *et al*., 2009; Wang *et al*., 2013).

3.3 Applied loads

The applied loads include the deadweight of the dam, the hydrostatic and sediment pressures of the reservoir, temperature load, and earthquake ground motion. Water depth is 205 m and the sediment level is 125 m above the dam base. Moreover, water pressure acting on the outlet and the gate thrust are considered in analyzing the pier sub-model. The thrust on the gate is 53,673 kN from static analysis; this value is multiplied by 1.2 in the dynamic analysis based on DL5073-2000 (2000). Fig. 7 presents the three components of the design earthquake ground motion, artificially generated based on the response spectrum specified in DL5073-2000 (2000). Peak ground accelerations are 0.557 g in the stream and cross-stream directions, and 0.371 g in the vertical direction.

Dynamic dam-reservoir interaction during earthquake ground shaking is modeled approximately using the generalized Westergaard added-mass model (Kuo, 1982; FERC, 1999), which takes into account the normal direction variation of the double-curvature upstream face. Therefore, both in the global model and the sub-model analyses, the hydrodynamic pressure acting on the upstream face is presented by the added mass.

Two earthquake input mechanisms are considered in the global analysis: the massless foundation model and the infinite foundation model. Radiation damping is neglected in the former but included in the latter. Seismic damage to the outlet pier is investigated for these cases in the following sections.

4 Earthquake damage analysis of the outlet pier (massless foundation)

In this section seismic damage of the outlet pier is analyzed based on the analysis results of the global model with a massless foundation. Considering that the accuracy of the nonlinear sub-model analysis was verified in a previous paper (Song *et al*., 2014), the verification results are not repeated herein. Therefore, four cases are analyzed straightforwardly: (1) plain pier, (2) anchored pier, (3) reinforced pier, and (4) anchored and reinforced pier. In the first case, no reinforcement is implemented in the analyzed pier. The effects of post-tensioned anchor cables and rebar are simulated in the second and third cases, respectively. The last case considers both post-tensioned anchor cables and rebar.

4.1 Plain pier

The damage distribution of the sub-model region for

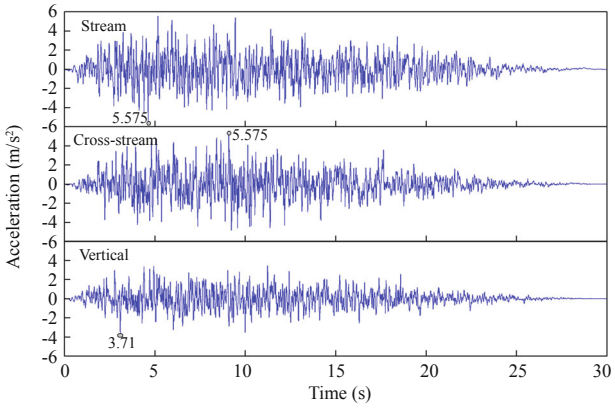

Fig. 7 Three components of the design ground motion

the plain pier is presented in Fig. 8. A strong earthquake results in heavy damage to the pier region. The damages are mainly concentrated at geometric mutation positions. (1) The connection interface between the dam body and the pier is completely damaged. The damage is more serious at the upper part of the connection interface, and the damage factor approaches to 1. (2) Two horizontal damage bands occur in the dam body. One damage band is along the spillway; the damage near the downstream orifice is most serious. Another damage band occurs above the pier, with a slightly lower damage factor. (3) On the pier itself, a horizontal cracking band occurs on both sidewalls at the upper part of the pier. In addition, the sidewall concrete is also damaged along the spillway surface, and the damage band extends almost all the way to the downstream surface of the pier. Both interfaces between the crossbeam and the sidewalls are seriously damaged.

Figure 9 shows the damage evolution in the simulation region following the design ground motion loading. The damage process of the plain pier can be summarized as follows.

(1) The damage caused by static loads at the upper connection interface extends to the upper edge of the downstream orifice during the beginning of ground motion at 0–2.5 s. Then, damage cracking extends

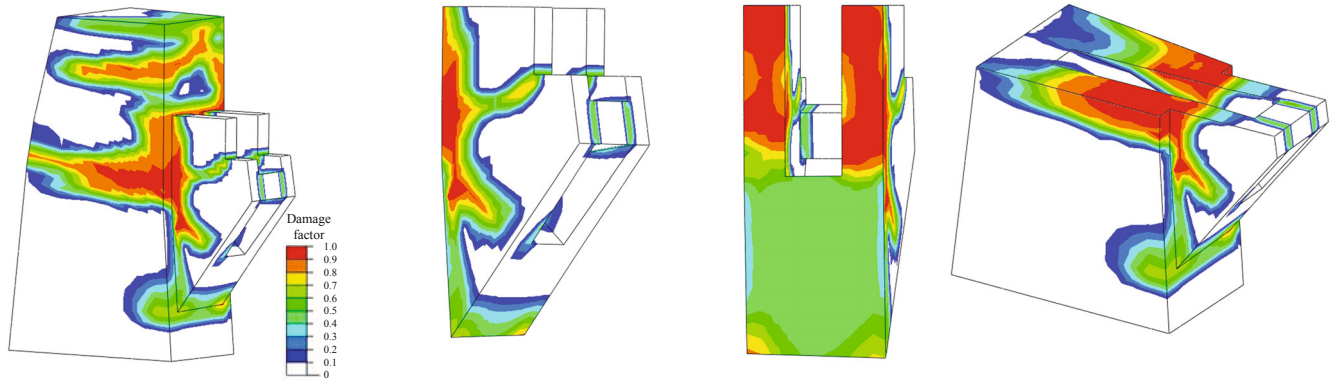

(a) Dam section and pier (b) Pier (c) Connection interface between the dam and the pier (d) Horizontal cross section at the upper edge of the crossbeam

Fig. 8 Damage distribution of the plain pier (massless foundation)

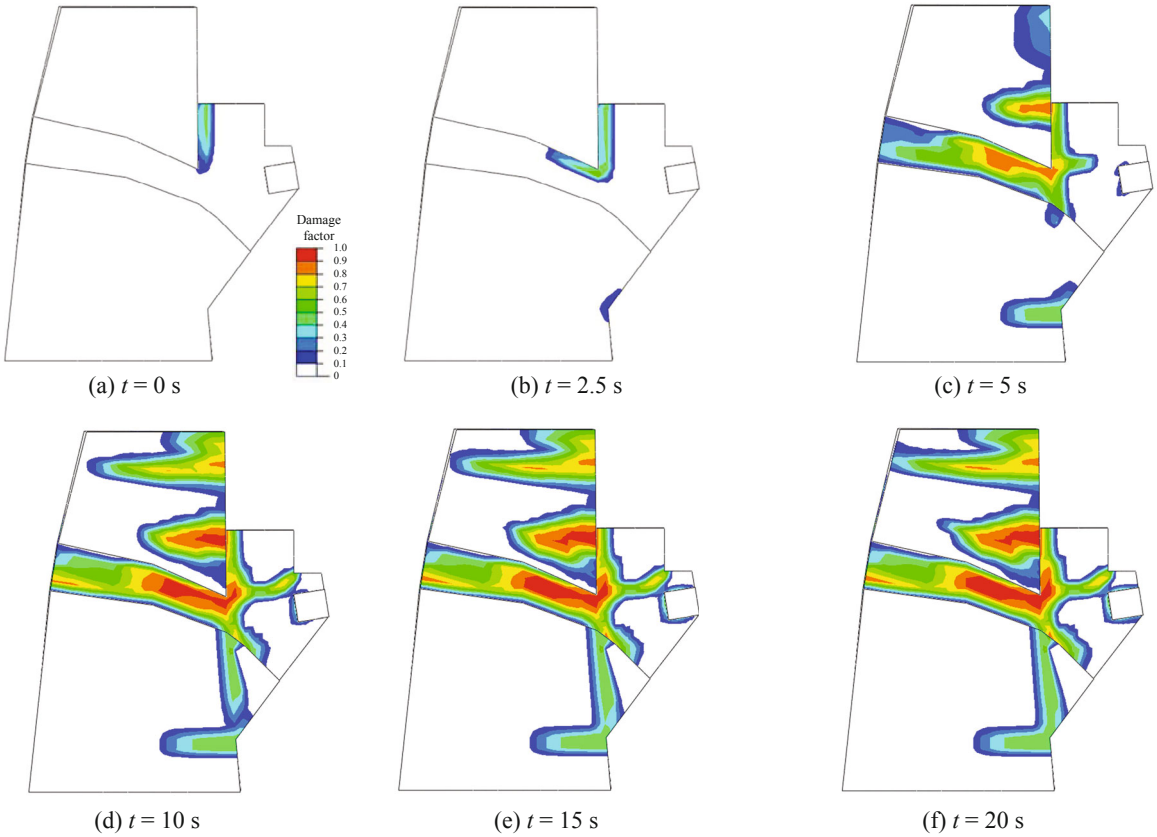

(a) t = 0 s (b) t = 2.5 s (c) t = 5 s

(d) t = 10 s (e) t = 15 s (f) t = 20 s

Fig. 9 Damage cracking process of the plain pier (massless foundation)

upstream along the spillway edges. Meanwhile, bottom edge of the pier is slightly damaged.

(2) Damage cracking progresses rapidly along geometric mutation positions when earthquake acceleration increases at 2.5–10 s. This situation leads to a number of severe damage bands in the dam body and the pier. Furthermore, the damage occurs throughout the connection interface between the dam body and the pier.

(3) No new cracking band is generated after earthquake peak acceleration at 10–20 s, but existing damage bands are slightly aggravated.

The aforementioned observations show that seismic damage is notable if the pier is plain concrete. Therefore, reinforcement measures are necessary.

4.2 Anchored pier

This subsection analyzes the effect of the post-tensioned anchor cables. The damage distribution with implementation of the anchor cables is shown in Fig. 10. The comparison between Figs. 8 and 10 shows that the anchor cables significantly reduce damage of the pier. (1) Damage distribution is evidently reduced at the connection interface between the dam body and the pier. No damage was observed at the lower part of the interface, as shown in Fig. 10 (b). This finding illustrates that the primary anchor cables effectively strengthen the connection between the outlet pier and the dam. (2) Both interfaces between the crossbeam and the sidewalls are hardly damaged, which illustrates that the secondary anchor cables effectively strengthen the connection between the crossbeam and the sidewalls. (3) A horizontal damage cracking band still occurs at the upper region of the pier. However, the damage factor is slightly reduced, and thus, damage does not occur throughout the damage band. (4) The sidewalls close to the spillway surface are still damaged, but the damage area and the damage factor are apparently reduced.

In general, the post-tensioned anchor cables effectively strengthen the outlet pier. However, several dangerous damage bands are still observed in the pier. Therefore, further seismic reinforcement measures should be taken.

4.3 Reinforced pier

This subsection investigates the effect of reinforcing bars on the dynamic damage of the outlet pier. Fig.11 presents the damage distribution of the outlet pier reinforced by rebars. It is observed that the damage distribution is similar to that in the plain pier case (Fig. 8), and thus the effect of the rebar is not significant. The damage of the dam body near the downstream orifice is alleviated by the reinforcing steel. The damage factor of the pier along the spillway surface is slightly reduced. However, the effect of the rebar is negligible

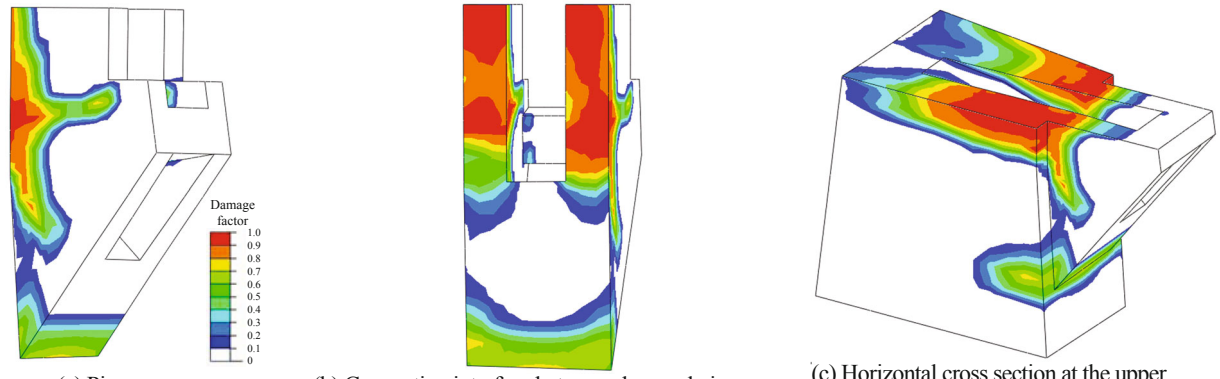

(a) Pier (b) Connection interface between dam and pier (c) Horizontal cross section at the upper edge of crossbeam

Fig. 10 Damage distribution of the anchored pier (massless foundation)

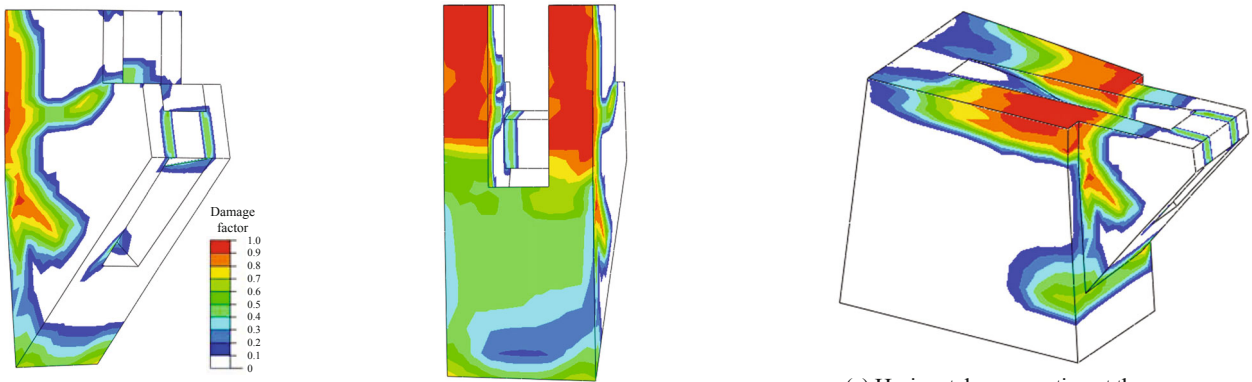

(a) Pier (b) Connection interface between dam and pier (c) Horizontal cross section at the upper edge of crossbeam

Fig. 11 Damage distribution of the reinforced pier (massless foundation)

in other parts. For example, there is almost no change to the damage at the connection interface between the dam body and the pier, and at the interfaces between the crossbeam and the sidewalls.

4.4 Anchored and reinforced pier

Both post-tensioned anchor cables and reinforcing bars are considered in this subsection. For this case, the damage distribution of the pier is shown in Fig. 12. It is apparent that the anchored and reinforced pier suffers much less damage than the plain pier (Fig. 8). In addition, comparison between Fig. 12 and Fig. 10 (the anchored pier case) shows that severely damaged areas are slightly reduced and the damage factor is decreased to a certain degree. These comparisons illustrate that the alleviation of the pier damage is mainly attributed to the post-tensioned anchor cables, and the effect of the rebar is insignificant as discussed in Subsection 4.3. The main reason for this phenomena is that the rebar ratio is too low to effectively strengthen the pier.

5 Effect of radiation damping on earthquake damage of the outlet pier

This section focuses on investigating the anchored and reinforced pier based on the dynamic responses from the global model with the infinite foundation. Therefore, the effect of radiation damping is considered.

Damage distribution is shown in Fig. 13 for the dam section with the pier. Comparison between Figs. 12 and 13 shows that radiation damping of the infinite foundation significantly reduces damage to the dam body and pier. For the dam body, the area with a damage factor over 0.5 is confined to within the vicinity of the downstream orifice. Damage only occurs at the upper part and bottom edge of the pier. Therefore, the pier is safe during strong earthquakes if radiation damping effect is included. However, the connection interface at the upper part of the pier is still broadly damaged because no post-tensioned anchor cable is employed in this region, as shown in Fig. 6(c). Therefore, increased reinforcement should be considered to enhance safety.

6 Conclusion

This study adopts the FE sub-model method to conduct seismic damage analyses of arch dam outlet piers. A 210-m-high arch dam in China is used as an example. Global analysis of the dam-foundation system considers nonlinearity of the dam concrete, nonlinearity

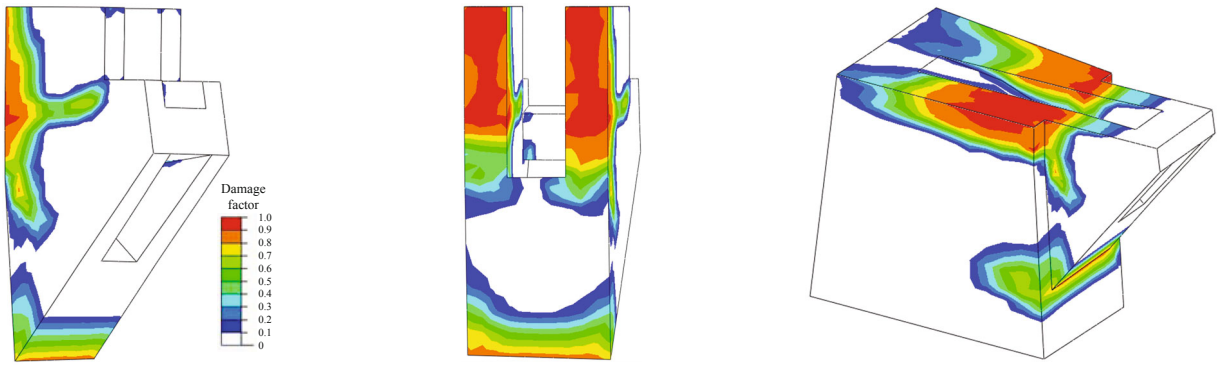

(a) Pier (b) Connection interface between dam and pier (c) Horizontal cross section at the upper edge of crossbeam

Fig. 12 Damage distribution of the anchored and reinforced pier (massless foundation)

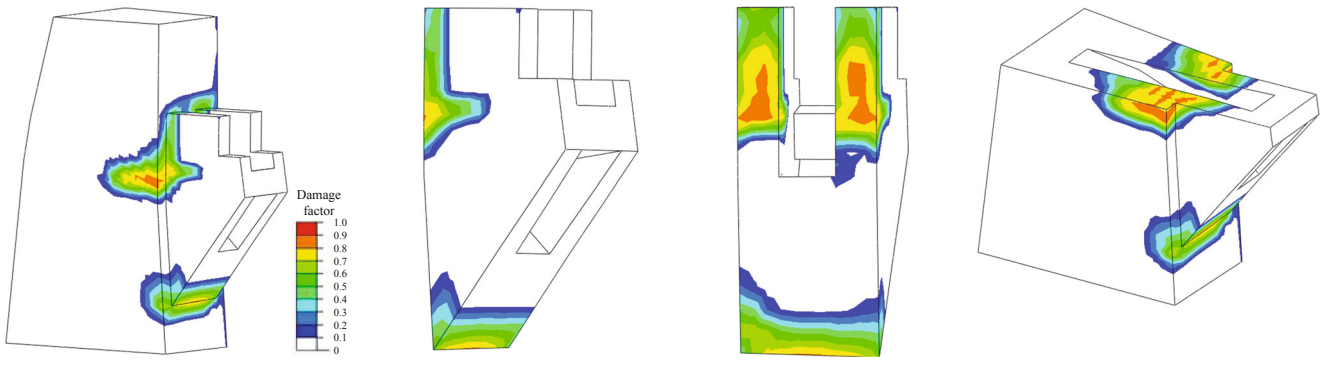

(a) Dam section and pier (b) Pier (c) Connection interface between the dam and the pier (d) Horizontal cross section at the upper edge of the crossbeam

Fig. 13 Damage distribution of the anchored and reinforced pier (infinite foundation)

of the contraction joints, and radiation damping of the infinite foundation. In the sub-model analysis, the outlet pier model accurately simulates the detailed structures and the reinforcement measures. Based on the sub-model analysis of the pier, the following conclusions are drawn.

(1) A plain pier may be heavily damaged during strong earthquakes. Damage develops along the geometric mutation positions, including the connection interface between dam body and pier, the spillway surface, and the interface between crossbeam and sidewalls.

(2) Post-tensioned anchor cables may effectively reduce the degree of damage to piers. Primary anchor cables effectively strengthen the connection between outlet pier and dam, whereas secondary anchor cables effectively strengthen the connection interface between crossbeam and sidewalls. However, rebar only reduces damage to the pier slightly.

(3) Radiation damping of the infinite foundation significantly reduces the damaged region of the pier. Damage is confined to a small region when radiation damping is considered. However, quantifying the damping behavior of the dam–foundation system is a challenging task and more efforts are needed in the future.

Acknowledgment

This research is financially supported by the National Natural Science Foundation of China (Nos. 51179093 and 91215301), the Specialized Research Fund for the Doctoral Program of Higher Education (No. 20130002110032), and Tsinghua University Initiative Scientific Research Program (No. 20131089285). The authors gratefully acknowledge these grants.

References

Alembagheri M and Ghaemian M (2013), "Damage Assessment of a Concrete Arch Dam through Nonlinear Incremental Dynamic Analysis," *Soil Dynamics and Earthquake Engineering*, **44**: 127−137.

Bayraktar A, Sevim B and Altunışık AC (2011), "Finite Element Model Updating Effects on Nonlinear Seismic Response of Arch Dam-reservoir-foundation Systems," *Finite Elements in Analysis and Design*, **47**(2): 85−97.

Bogdanovich AE and Kizhakkethara I (1999), "Three-dimensional Finite Element Analysis of Double-lap Composite Adhesive Bonded Joint Using Sub-modeling Approach," *Composites Part B: Engineering*, **30**(6): 537−551.

Chopra AK (2012), "Earthquake Analysis of Arch Dams: Factors to Be Considered," *Journal of Structural Engineering-ASCE*, **138**(2): 205−214.

Ciptokusumo J, Weide-Zaage K and Aubel O (2009), "Investigation of Stress Distribution in via Bottom of Cu-via Structures with Different via Form by Means of Sub-modeling," *Microelectronics Reliability*, **49**(9): 1090−1095.

Dassault Systèmes Simulia (2009), *ABAQUS Analysis User's Manual Version 6.9*, Providence, RI, USA.

DL5073-2000 (2000), *Specification of Seismic Design of Hydraulic Structures*, China Electric Power Press, Beijing, China.

Federal Energy Regulatory Commission (1999), "Arch Dams," in *Engineering Guidelines for the Evaluation of Hydropower Projects,* Chapter 11, Washington, DC 20426, USA.

Giglio M (1999), "FEM Sub-modelling Fatigue Analysis of a Complex Helicopter Component," *International Journal of Fatigue*, **21**(5): 445−455.

Hariri-Ardebili MA and Mirzabozorg HA (2013), "A Comparative Study of Seismic Stability of Coupled Arch Dam-foundation-reservoir Systems Using Infinite Elements and Viscous Boundary Models," *International Journal of Structural Stability and Dynamics*, **13**(6): 1350032.

Krishnan VR, Hui CY and Long R (2008), "Finite Strain Crack Tip Fields in Soft Incompressible Elastic Solids," *Langmuir*, **24**(24): 14245−14253.

Kuntiyawichai K and Burdekin FM (2003), "Engineering Assessment of Cracked Structures Subjected to Dynamic Loads Using Fracture Mechanics Assessment," *Engineering Fracture Mechanics*, **70**(15): 1991−2014.

Kuo J (1982), "Fluid-structure Interactions: Added Mass Computations for Incompressible Fluid," *Report No. UCB/EERC-82/09*, University of California Earthquake Engineering Research Center, Berkeley.

Lee JL and Fenves GL (1998), "Plastic-damage Model for Cyclic Loading of Concrete Structures," *Journal of Engineering Mechanics-ASCE*, **124**(3): 892−900.

Li DY, Tu J and Ouyang JH (2013), "Nonlinear Seismic Response Analysis on Xiluodu Arch Dam with Orifices and Piers," *Journal of Hydraulic Engineering*, **44**(11): 1366−1371. (in Chinese)

Li TC, Yan YY and Zhao LH (2008), "FEM Analysis of the Orifice Anti-seismic Reinforcement for High Arch Dam," *Proceedings of the 14th World Conference on Earthquake Engineering*, Paper No. S13-075, Beijing, China.

Liu J and Li B (2005), "A Unified Viscous-spring Artificial Boundary for 3-D Static and Dynamic Applications," *Science in China Series E: Engineering & Materials Science*, **48**(5): 570−584

Long YC, Zhang CH and JIN F (2008), "Numerical Simulation of Reinforcement Strengthening for High-Arch Dams to Resist Strong Earthquakes," *Earthquake Engineering and Structure Dynamics*, **37**: 1739−1761.

Lucht T (2009), "Finite Element Analysis of Three Dimensional Crack Growth by the Use of a Boundary Element Sub Model," *Engineering Fracture Mechanics*,

76(14): 2148−2162.

Mao C, Ricles J, Lu LW and Fisher J (2001), "Effect of Local Details on Ductility of Welded Moment Connections," *Journal of Structural Engineering*, **127**(9): 1036−1044.

Mircevska V, Nastev M, Hristovski V and Bulajic I (2014), "Arch Dam-fluid Interaction Considering Reservoir Topology," *Journal of Earthquake Engineering*, **18**(7): 1083−1101.

Pan JW, Zhang CH, Wang JT and Xu YJ (2009), "Seismic Damage-cracking Analysis of Arch Dams Using Different Earthquake Input Mechanisms," *Science in China Series E: Technological Sciences*, **52**: 518−529.

Song LF, Wu MX, Wang JT and Xu YJ (2014), "FE Sub-model Method for Seismic Response Analysis of Orifice Region in Arch Dams," *Journal of Hydroelectric Engineering*, **33**(3): 216−222. (in Chinese)

Wang GL, Pekau OA, Zhang CH and Wang SM (2000), "Seismic Fracture Analysis of Concrete Gravity Dams Based on Nonlinear Fracture Mechanics," *Engineering Fracture Mechanics*, **65**: 67−87.

Wang JT, Lv DD, Jin F and Zhang CH (2013), "Earthquake Damage Analysis of Arch Dams Considering Dam-water-foundation Interaction," *Soil Dynamics and Earthquake Engineering*, **49**: 64−74.

Zhang CH and Jin F (2008), "Seismic Safety Evaluation of High Concrete Dams Part I: State of the Art Design and Research," *Proceedings of the 14th World Conference on Earthquake Engineering*, Paper No. S13-080, Beijing, China.

Zhong H, Lin G, Li X and Li J (2011), "Seismic Failure Modeling of Concrete Dams Considering Heterogeneity of Concrete," *Soil Dynamics and Earthquake Engineering*, **31**: 1678−1689.